Article

Cell Stem Cell

m^{6}A RNA Methylation Is Regulated by MicroRNAs and Promotes Reprogramming to Pluripotency

Graphical Abstract

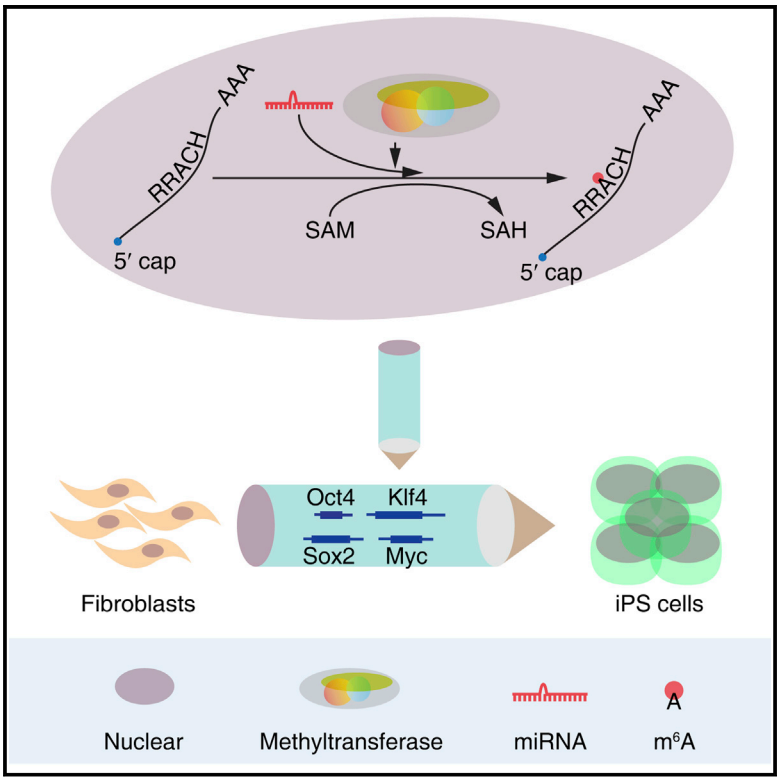

Authors

Tong Chen, Ya-Juan Hao, ..., Yun-Gui Yang, Qi Zhou

Correspondence

xjwang@genetics.ac.cn (X.-J.W.), ygyang@big.ac.cn (Y.-G.Y.), qzhou@ioz.ac.cn (Q.Z.)

In Brief

Zhou and colleagues show that formation of m^{6}A on mRNAs is regulated by miRNAs via a sequence pairing mechanism, and that in addition to differential distribution in pluripotent and differentiated cells, m^{6}A has a positive influence on reprogramming to pluripotency.

Highlights

- m^{6}A modification has gene- and cell-type-specific features
- m^{6}A modifications are enriched at miRNA targeting sites
- miRNAs regulate m^{6}A abundance by modulating METTL3 binding to mRNAs
- Increased m^{6}A formation promotes cell reprogramming to pluripotency

Accession Numbers

GSE52125

Chen et al., 2015, Cell Stem Cell *16*, 289–301
March 5, 2015
http://dx.doi.org/10.1016/j.stem.2015.01.016

Cell Stem Cell
Article

m^{6}A RNA Methylation Is Regulated by MicroRNAs and Promotes Reprogramming to Pluripotency

Tong Chen,[1,6,7] Ya-Juan Hao,[2,6,7] Ying Zhang,[3,7] Miao-Miao Li,[2,6,7] Meng Wang,[1] Weifang Han,[3,6] Yongsheng Wu,[2] Ying Lv,[2,6] Jie Hao,[3] Libin Wang,[3,6] Ang Li,[2,6] Ying Yang,[2,6] Kang-Xuan Jin,[2,6] Xu Zhao,[2,6] Yuhuan Li,[3] Xiao-Li Ping,[2,6] Wei-Yi Lai,[4] Li-Gang Wu,[5] Guibin Jiang,[4] Hai-Lin Wang,[4] Lisi Sang,[3,6] Xiu-Jie Wang,[1,*] Yun-Gui Yang,[2,*] and Qi Zhou[3,*]
[1]Key Laboratory of Genetic Network Biology, Collaborative Innovation Center of Genetics and Development, Institute of Genetics and Developmental Biology, Chinese Academy of Sciences, Beijing 100101, China
[2]Key Laboratory of Genomics and Precision Medicine, Collaborative Innovation Center of Genetics and Development, Beijing Institute of Genomics, Chinese Academy of Sciences, Beijing 100101, China
[3]State Key Laboratory of Reproductive Biology, Institute of Zoology, Chinese Academy of Sciences, Beijing 100101, China
[4]State Key Laboratory of Environmental Chemistry and Ecotoxicology, Research Center for Eco-Environmental Sciences, Chinese Academy of Sciences, Beijing 100085, China
[5]State Key Laboratory of Molecular Biology, Institute of Biochemistry and Cell Biology, Shanghai Institutes for Biological Sciences, Chinese Academy of Sciences, Shanghai 200031, China
[6]University of Chinese Academy of Sciences, Beijing 100049, China
[7]Co-first author
*Correspondence: xjwang@genetics.ac.cn (X.-J.W.), ygyang@big.ac.cn (Y.-G.Y.), qzhou@ioz.ac.cn (Q.Z.)
http://dx.doi.org/10.1016/j.stem.2015.01.016

SUMMARY

N^6-methyladenosine (m^{6}A) has been recently identified as a conserved epitranscriptomic modification of eukaryotic mRNAs, but its features, regulatory mechanisms, and functions in cell reprogramming are largely unknown. Here, we report m^{6}A modification profiles in the mRNA transcriptomes of four cell types with different degrees of pluripotency. Comparative analysis reveals several features of m^{6}A, especially gene- and cell-type-specific m^{6}A mRNA modifications. We also show that microRNAs (miRNAs) regulate m^{6}A modification via a sequence pairing mechanism. Manipulation of miRNA expression or sequences alters m^{6}A modification levels through modulating the binding of METTL3 methyltransferase to mRNAs containing miRNA targeting sites. Increased m^{6}A abundance promotes the reprogramming of mouse embryonic fibroblasts (MEFs) to pluripotent stem cells; conversely, reduced m^{6}A levels impede reprogramming. Our results therefore uncover a role for miRNAs in regulating m^{6}A formation of mRNAs and provide a foundation for future functional studies of m^{6}A modification in cell reprogramming.

INTRODUCTION

More than 100 types of post-transcriptional modifications have been identified in RNAs so far (Cantara et al., 2011; Globisch et al., 2011; He, 2010), among which N^6-methyladenosine (m^{6}A) RNA methylation is one of the most prevalent modifications of messenger RNAs (mRNAs) (Desrosiers et al., 1974; Wei et al., 1975). m^{6}A accounts for about 50% of total methylated ribonucleotides and is present in 0.1%–0.4% of all adenosines in total cellular RNAs (Desrosiers et al., 1974; Wei et al., 1975). In vivo, the formation of m^{6}A is catalyzed by a multicomponent methyltransferase complex with at least three proteins, namely methyltransferase-like 3 (METTL3), METTL14, and Wilms' tumor 1-associating protein (WTAP) (Bokar et al., 1997; Finkel and Groner, 1983; Liu et al., 2014; Ping et al., 2014; Schwartz et al., 2014; Wang et al., 2014b). The m^{6}A modification can be removed by RNA demethylases, of which the two known ones are fat mass and obesity-associated protein (FTO) and alkylated DNA repair protein alkB homolog 5 (ALKBH5) (Jia et al., 2011; Zheng et al., 2013). So far, two YTH (YT521-B homology)-domain containing proteins, YTHDF2 and YTHDC1, have been identified to specifically recognize m^{6}A-modified RNAs (Dominissini et al., 2012; Xu et al., 2014; Zhu et al., 2014).

In general, m^{6}A modification can be detected in the mRNAs of over 7,000 genes in mammalian cells, and it tends to occur at the consensus RRACH motif (R = G or A; H = A, C, or U) (Bodi et al., 2010; Dominissini et al., 2012; Harper et al., 1990; Meyer et al., 2012; Wei and Moss, 1977). On average, the frequency of m^{6}A modification is about one peak per 2,000 nucleotides (nts), but there are also some regions with clustered m^{6}A peaks (Dominissini et al., 2012; Kane and Beemon, 1985; Meyer et al., 2012). Strong enrichment of m^{6}A modification has been found near the stop codons of mRNAs (Dominissini et al., 2012; Meyer et al., 2012).

Although the existence of m^{6}A does not change the coding capacity or base pairing of adenine with uracil or thymine, it may block the nonstandard A:G base pairing and influence RNA structures (Dai et al., 2007). The presence of m^{6}A may also affect the expression level, translation efficiency, nuclear retention, splicing, and stability of mRNAs (Camper et al., 1984; Finkel and Groner, 1983; Fustin et al., 2013; He, 2010; Hess et al., 2013; Liu et al., 2014; Ping et al., 2014; Schwartz et al., 2013; Tuck et al., 1999; Wang et al., 2014a, 2014b; Zhao et al., 2014; Zheng et al., 2013). Deficiency of m^{6}A

formation has been proven to affect circadian rhythm, cell meiosis, and embryonic stem cell (ESC) proliferation, and thus it is implicated in obesity, cancer, and other human diseases (Batista et al., 2014; Dominissini et al., 2012; Geula et al., 2015; He, 2010; Liu and Jia, 2014; Liu et al., 2013; Machnicka et al., 2013; Meyer et al., 2012; Niu et al., 2013; Sibbritt et al., 2013). However, the regulatory mechanisms of m^6A formation and the function of m^6A in regulating cell reprogramming are still largely unknown.

Here we examined the transcriptome-wide distribution of m^6A modification in mouse ESCs, induced pluripotent stem cells (iPSCs), neural stem cells (NSCs), and testicular sertoli cells (SCs). Our results identified the difference in m^6A distribution between pluripotent and differentiated cell types. We discovered that the m^6A formation of mRNAs is regulated by microRNAs (miRNAs) via a sequence pairing mechanism, and we revealed m^6A as a positive regulator for cell reprogramming to pluripotency.

RESULTS

General Features of m^6A Distribution in Mouse Pluripotent and Differentiated Cell Lines

To investigate the features and distribution dynamics of mRNA m^6A modification in different cell types, we performed m^6A-seq using mouse ESCs, iPSCs, NSCs, and SCs. In total, 33,000–43,000 m^6A-enriched regions, also known as m^6A peaks, were identified on mRNAs of 7,000–8,000 expressed genes in each cell type. Using m^6A-qRT-PCR, 13 out of 15 randomly selected m^6A peaks were verified in all cell types (Figures S1A and S1B), implying a high authenticity of our data. Genes encoding transcripts with m^6A modifications involved in many essential biological processes, including transcription regulation, chromatin modification, cell cycle control, apoptosis, etc., among which transcripts encoding proteins for DNA binding activity were identified as the most significantly enriched group (counted for over 10% of m^6A-modified genes) (Figure S1C, Table S1, and Table S2).

Similar to previous reports (Dominissini et al., 2012; Meyer et al., 2012), we also observed a tendency toward m^6A distribution in the coding sequence (CDS) region of mRNAs, with a strong enrichment around the translation termination sites (TsTS) in all four examined cell types (Figure S1D). Transcripts of majority genes (ESCs, 77%; iPSCs, 72%; NSCs, 63%; SCs, 74%) each harbored fewer than five m^6A peaks, yet there were transcripts of some genes (ESCs, 9%; iPSCs, 4%; NSCs, 12%; SCs, 6%) with over 50% of their lengths covered by m^6A peaks (Figure S1E); we thus named these "m^6A high-coverage transcripts." The length of these m^6A high-coverage transcripts did not differ significantly from that of the overall transcripts, and some of these transcripts encoded proteins involved in the regulation of processes essential for the maintenance of cell-type specific features, such as neuron differentiation and development in NSCs (Table S3).

Common and Cell-Type-Specific m^6A Modification

Using the Shannon-entropy-based method (Xie et al., 2013), we identified a total of 8,558 genes with stable expression in all examined cell types (Table S4). Among them, only transcripts of 3,880 genes had m^6A modifications in all samples and were enriched in essential biological processes (Figure 1A and Table S4). On the other hand, transcripts of 1,087 stably expressed genes had no m^6A modification in any examined cell type, and the functions of these genes tended to relate to the synthesis and functional establishment of proteins (Figure 1B and Table S4).

To study the m^6A modification profiles across cell types, we further divided each transcript into TcSS (transcription start sites), 5′ UTR, CDS, TsTS (translation termination sites), and 3′ UTR regions and compared the m^6A distribution profile within each region. m^6A modifications in CDS and TsTS regions were more conserved across cell types than those in other regions, with about 50% transcripts having m^6A modifications in the CDS and TsTS regions in all examined cell types; yet, only less than 5% of m^6A modifications in the TcSS and 5′ UTR regions were conserved across cell types (Figures 1C and 1D and Table S4). At the transcript level, only 437 (11% of 3,880) transcripts had consistent m^6A distribution profiles in all examined samples (Figure 1C), and the rest of the transcripts (3,443; 89% of 3,880) had variable m^6A peaks in at least two cell types (Figure 1D).

A total of 1,695 genes were identified as cell-type-specifically expressed, of which 998 genes had transcripts with m^6A modifications (Figure 1E and Table S5). In addition, among the 8,558 genes with stable expression in all cell types, the transcripts of 877 genes had cell-type-specific m^6A modifications. Gene ontology analysis revealed transcripts with cell-type-specific m^6A modifications involved in many cell-type-specific biological processes, such as stem cell maintenance and developmental regulation in ESCs and iPSCs, as well as neuron differentiation and forebrain development regulation in NSCs (Table S5). As expected, many known cell-type specific markers were among these genes, including key transcription factors essential for specific features of each cell type, such as *Oct4*, *Nanog*, and *DPPA2* for ESCs and iPSCs; *POU3F2* and *ROBO2* for NSCs; and *DHH* and *Sox8* for SCs (Figures 1E and S1F).

m^6A Peaks Are Enriched at miRNA Target Sites

To investigate the sequence features of m^6A methylation sites, we performed motif search among m^6A regions of all cell types. More than 87% of identified m^6A peaks contained the previously reported RRACH motif, with GGACU as the most frequent motif in all examined cell types (Figure 2A). The enrichment of the RRACH motif among m^6A peaks was significantly higher than that among the control peaks ($p < 2.2e{-}16$, Fisher's exact test). In addition, we also identified a few other motifs (ESCs: 15; iPSCs: 9; NSCs: 8; SCs: 12) within 87%–99% of m^6A peak regions (Figures S2A–S2D). Intriguingly, we found that the RRACH motif and over two-thirds (67%–89%, depending on the cell type) of the identified motifs were reversely complementary to the seed sequences (5′ 2-8 nucleotides) of one or more miRNAs with at most 1 nt mismatch, indicating that the m^6A peak regions may be targeted by miRNAs (Figures 2B and 2C and S2A–S2D). Further analysis revealed that 92%–96% of the m^6A peaks could pair with miRNAs with relatively strict alignment criteria. In particular, the RRACH motif region of m^6A peaks could potentially pair with 482 miRNAs. The enrichment of miRNA binding sites

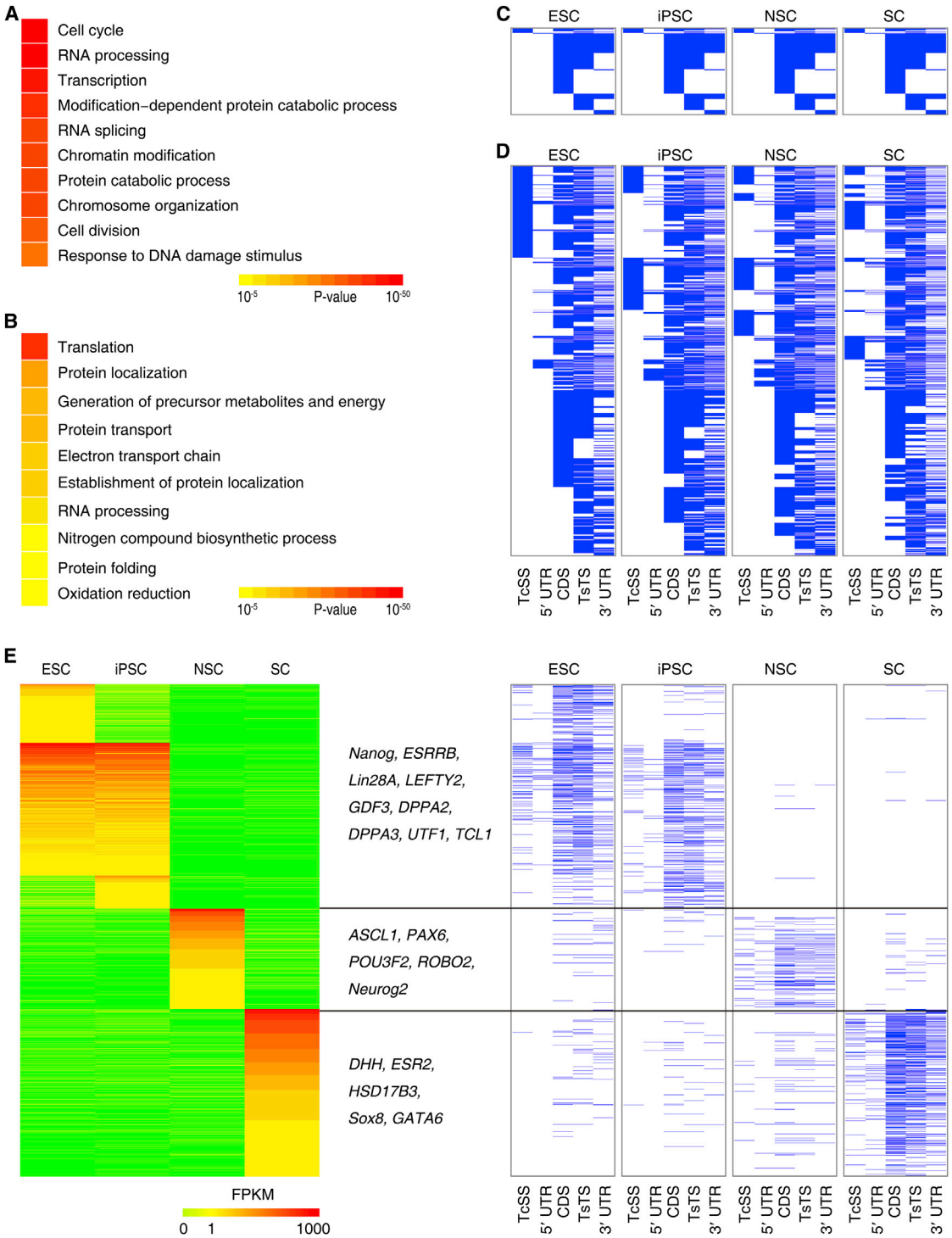

Figure 1. Dynamic m^{6}A Modification among Cell Types

(A and B) Representative Gene Ontology (GO) terms of the biological process category enriched by transcripts stably expressed in all cell types with (A) or without (B) m^{6}A modifications.

(C and D) Distribution of m^{6}A peaks along cell-type-consistently expressed transcripts with identical (C) or variable (D) modification profiles among cell types. Each horizontal line represents one transcript. Blue lines represent m^{6}A peaks within each sequence region. TcSS, transcription start sites; 5′ UTR, 5′ untranslated region; CDS, coding sequence; TsTS, translation termination sites; 3′ UTR, 3′ untranslated region.

(E) Expression profile of cell-type-specifically expressed transcripts (left) and the distribution of m^{6}A peaks on each transcript (right). Blue lines represent m^{6}A peaks within each sequence region. Names of selected cell-type-specific genes are listed.

See also Figure S1, Table S1, Table S2, Table S3, Table S4, Table S5, and Table S6.

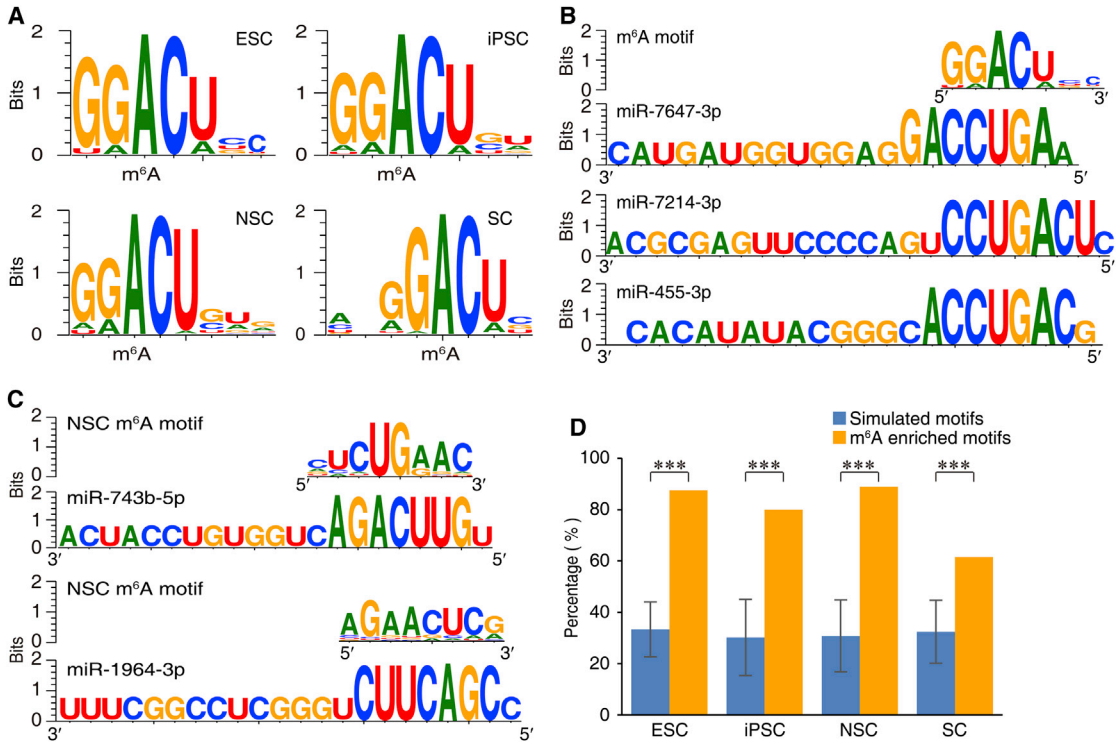

Figure 2. m^{6}A Peaks as Putative miRNA Target Sites

(A) The most common sequence motif among m^{6}A peaks in each cell type.

(B) Pairing situation between the most common m^{6}A motif with the sequences of corresponding miRNAs. Full-size letters in miRNAs represent "seed sequences."

(C) Pairing situation of two selected m^{6}A motifs in NSCs with corresponding miRNAs. Full-size letters in miRNAs represent seed sequences.

(D) The percentage of m^{6}A-enriched motifs targeted by miRNAs among all m^{6}A-enriched motifs versus the percentage of simulated motifs targeted by miRNAs among all simulated motifs. Error bars represent SD of 500 simulated experiments.

***p < 2.2e−16 by Student's t test. See also Figure S2 and Table S6.

among m^{6}A enriched motifs was remarkably higher than those of the randomly simulated motifs (Figure 2D).

To investigate whether these m^{6}A-targeting miRNAs were indeed expressed in corresponding cells, we quantified miRNA expression using small RNA-seq in ESCs. Of the 1,866 m^{6}A-targeting miRNAs, 818 were detected to be expressed in ESCs. These expressed miRNAs had a significant tendency to target m^{6}A peaks as compared to control peaks (71% versus 39%, p < 2.2e−16, Fisher's exact test). The consistency between small RNA-seq data and cellular miRNA abundance was validated by qRT-PCR on 12 randomly selected miRNAs (including 2 cell-type-specific ones) (Figures S2E and S2F). Using the same criteria, 75% of m^{6}A peaks were identified as potential targets of expressed miRNAs in HeLa cells using the published m^{6}A data (Wang et al., 2014a), indicating the conservation of miRNA regulation on m^{6}A between human and mouse.

Formation of m^{6}A Depends on Dicer, but Not Argonaute

To investigate whether miRNAs were indeed involved in the regulation of m^{6}A, we examined the effects of key miRNA biogenesis proteins on cellular m^{6}A abundance. Knocking down *Dicer*, the endonuclease responsible for producing mature miRNAs, significantly reduced cellular m^{6}A abundance in both mouse NSCs (Figures 3A and 3B and S3A) and human HeLa cells (Figures 3D and 3E and S3B). Conversely, overexpressing *Dicer* increased the m^{6}A modification level (Figures 3G, 3H, 3J, 3K, and S3C). In all these experiments, expected Dicer and miRNA expression changes were detected, whereas the protein abundance of neither m^{6}A methyltransferase METTL3 nor demethylases FTO and ALKBH5 were affected (Figures 3C, 3F, 3I, 3L, and S3D), suggesting that Dicer-induced m^{6}A abundance change was not achieved by the alteration of the quantity of m^{6}A methyltransferase or demethylases in cells.

Argonaute (AGO) proteins are the key components of known miRNA functional pathways and mediate the binding of miRNAs to their target mRNAs (Bartel, 2004; Cenik and Zamore, 2011; Meister, 2013; Rand et al., 2005). We further examined whether AGO proteins participate in the regulation of m^{6}A formation. The genomes of human and mouse each encode four types of AGO clade proteins (AGO1–AGO4) with miRNA binding ability (Cenik and Zamore, 2011; Meister, 2013). Unexpectedly, knocking down individual AGO expression in HeLa cells had no effect on m^{6}A abundance (Figures S3E–S3G). To avoid functional redundancy, we further used mixed siRNAs to knock down all four *AGO* genes in mouse NSCs and human HeLa cells. Neither

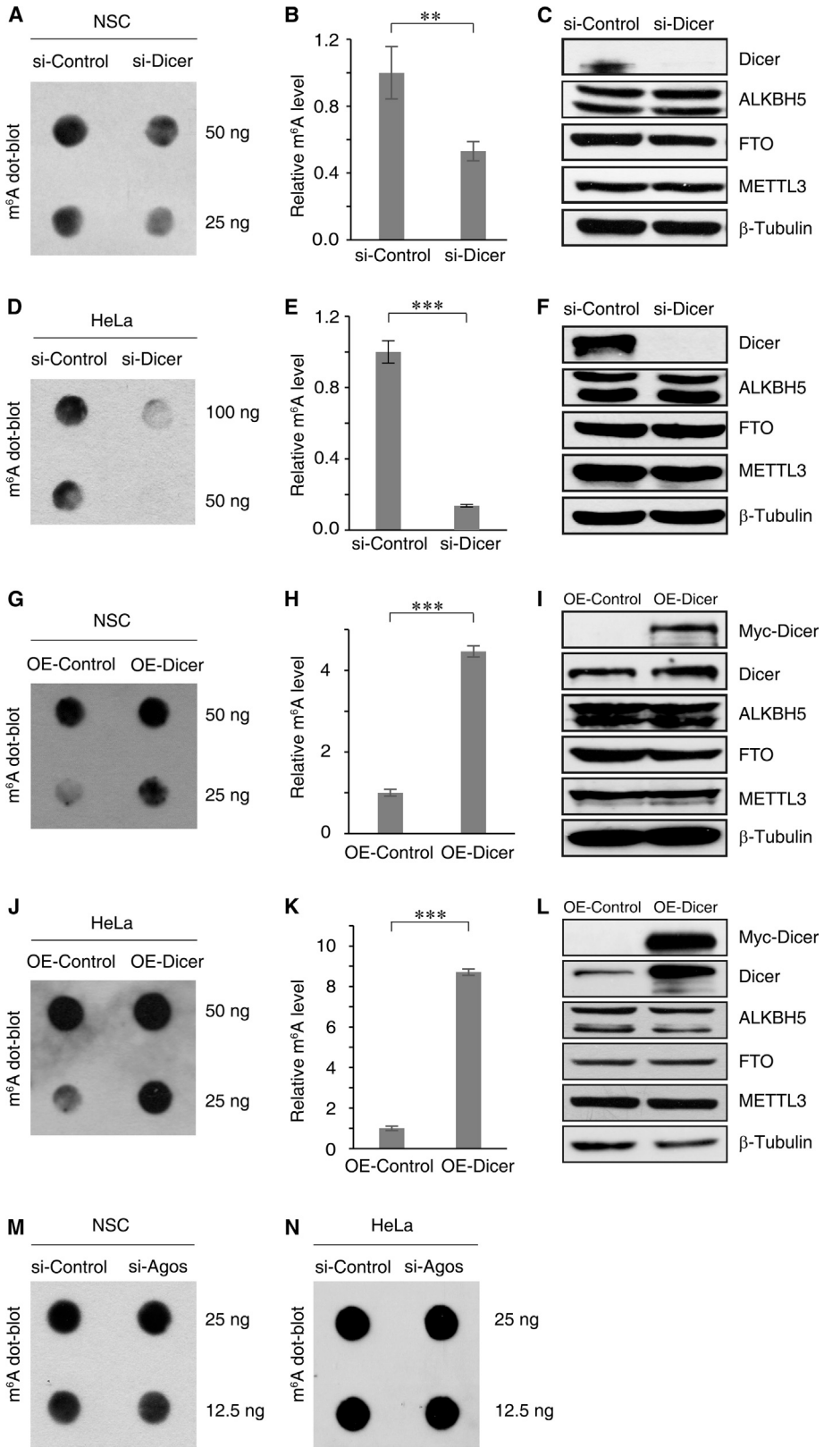

(legend on next page)

experiment resulted in an exhibited abundance change of total m^{6}A (Figures 3M, 3N, and S3H–S3K), ruling out the involvement of AGO proteins in regulating m^{6}A formation.

miRNAs Affect the Abundance of m^{6}A at Corresponding Target Sites

To investigate whether miRNAs indeed function in regulating m^{6}A formation, we overexpressed a few randomly selected miRNAs with sequences pairing to m^{6}A peak regions in mouse NSCs, and we observed significantly increased m^{6}A abundance at the corresponding miRNA target sites (Figure 4A upper panel and Figures S4A and S4C). Conversely, repressing the expression of miRNAs by antagomirs significantly reduced m^{6}A abundance (Figure 4B left panel and Figures S4E and S4G). The expression of target genes (Figure 4A lower panel and Figure 4B right panel) as well as m^{6}A methyltransferase METTL3 and demethylases ALKBH5 and FTO (Figures S4B, S4D, S4F, and S4H) remained unaffected in these experiments, suggesting that the abundance change of m^{6}A was not caused by altered expression of target genes or m^{6}A regulating enzymes. Consistently, overexpression or knockdown miRNAs (miR-423-3p and miR-1226-3p) also increased or decreased m^{6}A abundance in human HeLa cells (Figures 4C and S4I).

To investigate whether miRNAs are capable of mediating the ab initio formation of m^{6}A, we mutated three nucleotides in the 5′ 2-8 nt region (seed sequence of miRNAs) of four miRNAs, namely miR-330-5p, miR-668-3p, miR-1224-5p, and miR-1981-5p, to make the mutated miRNAs pairing with mRNA regions originally without m^{6}A peaks. Consistent results from six individual loci in mouse NSCs demonstrated that overexpression of the mutated miRNAs indeed caused the formation of m^{6}A at the designed target sites, whereas regions not targeted by the mutated miRNAs had no m^{6}A abundance change (control: KIF1B and control:SCD2) (Figures 4D and S4J). Due to the mutations, some m^{6}A peaks originally targeted by endogenous miRNAs were no longer targeted by the mutated ones, and no m^{6}A abundance change was detected at these sites either (i.e., control:SSRP1 was targeted by miR-1224-5p, but not its mutant) (Figures 4D and S4J). These results demonstrated that miRNAs are capable of inducing de novo m^{6}A methylation via a sequence-dependent manner.

miRNAs Modulate METTL3 Binding to mRNAs

The ab initio induction of m^{6}A methylation by mutated miRNAs drove us to speculate that miRNAs may regulate the interaction between METTL3 and mRNAs. To test this hypothesis, we first examined whether modulating *Dicer* expression could affect the subcellular localization of METTL3, as it has been shown that METTL3 locates and functions at nuclear speckles (Liu et al., 2014; Ping et al., 2014; Wang et al., 2014b). Knocking down *Dicer* significantly reduced the nuclear staining density of METTL3 in human HeLa cells (Figures 5A and 5B). Further examination using ASF (a nuclear speckle marker) staining revealed that the nuclear speckle localization of METTL3 was indeed disrupted in *Dicer* knockdown HeLa cells (Figure 5C), whereas the METTL3 abundance in both nucleus and cytoplasm almost remained unchanged (Figures 5D and S5A). Co-immunoprecipitation assay revealed that Dicer did not associate with METTL3 (Figures S5B and S5C), ruling out a potential physical interaction between METTL3 and Dicer. Taken together, these results indicated that Dicer regulates the nuclear speckle localization of METTL3.

We next performed Photoactivatable-Ribonucleoside-Enhanced Crosslinking and Immunoprecipitation (PAR-CLIP) to examine the amount of RNA associated with METTL3. Intriguingly, upon Dicer depletion, the amount of RNA crosslinked to Myc-tagged METTL3 was significantly reduced in human HeLa cells (Figures 5E and 5F). To further investigate whether the binding of METTL3 on mRNAs could be altered by individual miRNAs processed by Dicer, we performed an RNA immunoprecipitation (RIP) assay with METTL3 antibody to precipitate endogenous METTL3 and its associated mRNAs from HeLa cells, after the overexpression of miR-423-3p and miR-1226-3p or their antagomirs. In concert with the results of Dicer manipulation, overexpressing miRNAs significantly increased the amount of mRNAs associated with METTL3, whereas downregulating miRNA abundance by antagomirs significantly reduced METTL3 binding on mRNAs (i.e., DGCR2 and TUBB4B, targeted by miR-423-3p and miR-1226-3p, respectively) in HeLa cells (Figures 5G and 5H). Consistently, the amounts of METTL3-crosslinked total RNAs (Figure 5I) and mRNAs (i.e., TCF4 and RPS13) targeted by designed miRNAs (Figures 5J and S5D) were also altered in mouse NSCs when manipulating Dicer or corresponding miRNAs, respectively. In both the mouse and human experiments, the abundance of METTL3-bound mRNAs not targeted by the designed miRNAs was not altered (i.e. TXNRD1 and CTNNA1 in Figure 5G; EEF1A1 in Figure 5J). Collectively, these results showed that miRNAs regulate the m^{6}A methyltransferase activity of METTL3 by modulating its binding to mRNAs.

m^{6}A Actively Promotes Cell Reprogramming Efficiency

To investigate whether m^{6}A of mRNAs plays roles in cell fate determination, we resorted to the iPSC technology to examine

Figure 3. Cellular m^{6}A Abundance Is Regulated by Dicer, but Not AGO

(A and D) m^{6}A dot blot of the control and *Dicer* knockdown mouse NSCs (A) and human HeLa cells (D). (B and E) Quantification of m^{6}A abundance in (A) and (D), respectively. (C and F) Western blot analysis for protein abundance of miRNA processing enzyme Dicer and m^{6}A methyltransferase (METTL3) and demethylases (FTO and ALKBH5) in mouse NSCs (C) and human HeLa cells (F) transfected with siRNAs for *Dicer* for 48 hr. β-Tubulin is used as a loading control. (G and J) m^{6}A dot blot of the control and *Dicer* overexpression mouse NSCs (G) and human HeLa cells (J). (H and K) Quantification of m^{6}A abundance in (G) and (J), respectively. (I and L) Western blot analysis for protein abundance of Dicer, METTL3, FTO, and ALKBH5 in mouse NSCs (I) and human HeLa cells (L) transfected with vectors containing exogenous Myc-tagged *Dicer* (Myc-Dicer). Endogenous Dicer expression is labeled as "Dicer." β-Tubulin is used as a loading control. (M and N) Dot blot assay showing the amount of m^{6}A in the control and *Ago1–4* knockdown mouse NSCs (M) and human HeLa cells (N).

Values and error bars in all bar plots represent the mean and standard deviation (SD) of three independent experiments. $^{**}p < 0.01$ and $^{***}p < 0.001$ by Student's t test. See also Figure S3 and Table S6.

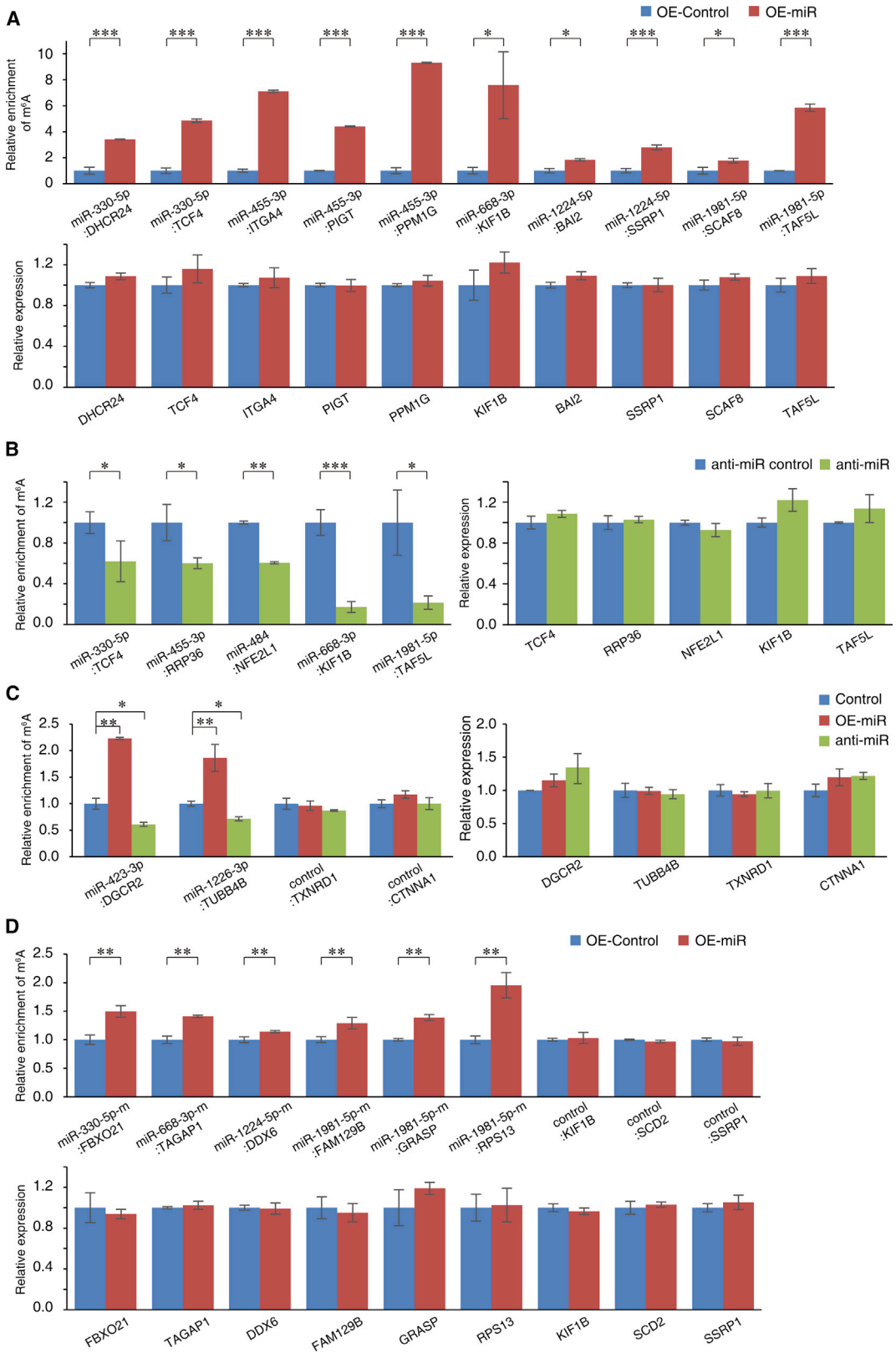

(legend on next page)

the effects of m^{6}A on cell reprogramming. We first overexpressed human Myc-*METTL3* into mouse embryonic fibroblasts (MEFs) expressing the four Yamanaka factors (*Oct4*, *Sox2*, *Klf4*, and *c-Myc*). Overexpression of *METTL3* in MEFs increased m^{6}A abundance (Figure S6A left panels and Figure S6B) and significantly improved the reprogramming efficiency, with the number of obtained iPSC colonies (Oct4:: GFP-positive and AP-positive) in the METTL3 overexpression experiment almost double that of the control (Figures 6A and 6B). Enhanced expression of key pluripotent factors, such as *Oct4*, *Sox2*, and *Nanog*, was also observed in METTL3-overexpressing cells (Figure 6C). Conversely, inhibiting m^{6}A formation by knocking down *METTL3* expression using siRNAs during the reprogramming process resulted in reduced iPSC colony numbers as well as decreased pluripotent gene expression (Figures 6D–6F, Figure S6A right panels, and Figure S6C). Decreased m^{6}A abundance and iPSC colony numbers were also observed with the addition of cycloleucine, a competitive inhibitor of methionine adenosyltransferase (Finkel and Groner, 1983), during the reprogramming process (Figures S6D–S6F). Furthermore, overexpression of human Myc-*METTL3* insensitive to mouse METTL3 siRNAs in mouse *METTL3* knockdown MEFs successfully rescued the reprogramming efficiency (Figures 6D–6F, Figure S6A right panels, and Figure S6C). These data indicated that m^{6}A is required for MEF reprogramming to pluripotency and can promote the reprogramming efficiency.

DISCUSSION

Increasing lines of evidence have shown that m^{6}A modification may play pivotal physiological functions in regulating RNA metabolism and various biological processes (Bodi et al., 2012; Bokar, 2005; Fustin et al., 2013; Geula et al., 2015; Jia et al., 2011; Liu et al., 2014; Ping et al., 2014; Schwartz et al., 2013; Wang et al., 2014a, 2014b; Zhao et al., 2014; Zheng et al., 2013; Zhong et al., 2008). With the advances of m^{6}A-seq technology, the basic features of m^{6}A modification have been characterized in some tissues and cell lines of mouse and human (Batista et al., 2014; Dominissini et al., 2012; Fustin et al., 2013; Meyer et al., 2012; Schwartz et al., 2013; Wang et al., 2014b). Yet the dynamics of m^{6}A among different cell types and its regulatory mechanisms are still largely unknown. Here we reported cross cell-type comparison of m^{6}A profiles using mouse pluripotent and differentiated cell lines. We identified transcripts with cell-type-dependent common or specific m^{6}A modifications and revealed the dynamic changes of m^{6}A across cell types on some consistently expressed transcripts. These results will provide clues for further functional studies of m^{6}A modification.

miRNAs are a group of important post-transcriptional regulators in eukaryotes. Two previous reports discussed that the presence of m^{6}A may affect the binding of miRNAs to target mRNAs (Meyer et al., 2012; Wang et al., 2014b), but whether miRNAs have direct regulatory roles in the formation of m^{6}A has not been explored yet. Here, we showed that the overall cellular m^{6}A abundance and m^{6}A on individual mRNAs can be altered by the modulation of the expression of the miRNA biogenesis enzyme Dicer or miRNAs. In addition, overexpression of miRNA mutants creates m^{6}A methylation ab initio on originally unmethylated mRNA sequences via a sequence-dependent mechanism. We have further found that the function of miRNAs in regulating m^{6}A is achieved by the mediation of the binding of m^{6}A methyltransferase METTL3 to mRNAs. These results reveal the functions of miRNAs in regulating the formation of m^{6}A, and they also partially explain the site selection mechanism of m^{6}A.

As the key effector proteins of the miRNA functional cascade, AGO proteins have been shown to bind to miRNAs and help miRNAs to execute their functions. However, our results showed that in both human and mouse cells, none of the AGO1–AGO4 proteins were involved in miRNA-mediated m^{6}A regulation. It is likely that miRNAs associate with proteins other than AGOs to regulate m^{6}A formation. Given the presence of a large number of RNA binding proteins with unknown functions, finding the miRNA binding proteins involved in m^{6}A modification remains challenging and needs further investigation.

The physiological roles of m^{6}A modification in cell fate determination are still largely unknown so far. By examining the functions of m^{6}A in regulating cell reprogramming using the iPSC technology, we have revealed a positive role of m^{6}A in regulating cell reprogramming. Such effects were accompanied by altered expression of key pluripotent factors, such as *Oct4*, *Sox2*, and *Nanog*. Consistently, two recent studies reported that proper formation of m^{6}A is required for maintaining the ground state of human and mouse ESCs (Batista et al., 2014; Geula et al., 2015), which is in concert with the function of m^{6}A in promoting the iPSC process identified in this work. All these suggested that proper m^{6}A formation is essential for differentiated cells to regain pluripotent property.

In summary, our study provided the m^{6}A profiles in mouse pluripotent and differentiated cell lines and identified the cell-type-specific and several other features of m^{6}A modification. We have demonstrated that miRNAs are involved in the

Figure 4. m^{6}A Is Regulated by miRNAs

(A) qRT-PCR showing the m^{6}A changes at predicted target sites of overexpressed miRNAs (upper panel) and the expression changes of the m^{6}A modified target genes (lower panel) in mouse NSCs.

(B) qRT-PCR showing the m^{6}A changes at predicted target sites of selected miRNAs (left panel) and the expression changes of the m^{6}A modified target genes (right panel) in mouse NSCs with selected miRNAs knocked down by antagomirs.

(C) qRT-PCR showing the m^{6}A changes at predicted target sites of overexpressed or repressed miRNAs (left panel) and the expression changes of the m^{6}A modified target genes (right panel) in human HeLa cells.

(D) qRT-PCR showing the m^{6}A changes at predicted target sites of four artificial miRNAs (upper panel) and the expression changes of the m^{6}A modified target genes (lower panel) in mouse NSCs.

Values and error bars in all bar plots represent the mean and SD of three independent experiments. *$p < 0.05$, **$p < 0.01$, and ***$p < 0.001$ by Student's t test. See also Figure S4 and Table S6.

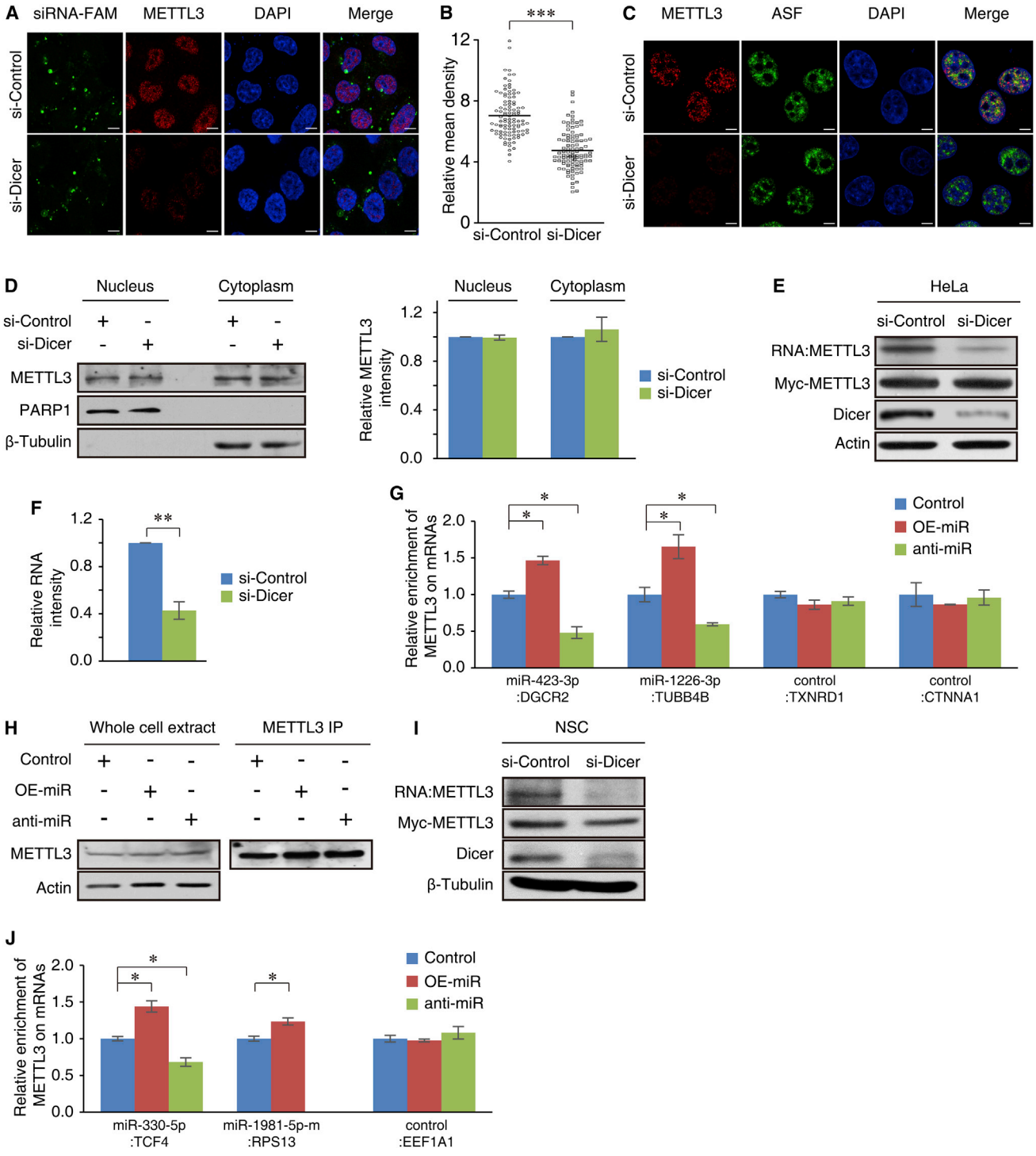

Figure 5. miRNAs Affect METTL3 Binding to RNAs

(A) Immunofluorescence analysis of FAM-labeled *Dicer*-siRNA (green), METTL3 (red), and DAPI (blue, cell nuclei) in *Dicer* knockdown and control HeLa cells. Scale bar, 7.5 μm.

(B) Quantification of fluorescence intensity of METTL3 in (A). n = 101 cells for each sample.

(C) Immunofluorescence analysis of METTL3 (red), ASF (green, nuclear speckles), and DAPI (blue, cell nuclei) in *Dicer* knockdown and control HeLa cells. Scale bar, 5 μm.

(D) Western blot (left panel) and quantitative analysis (right panel) of nuclear and cytoplasmic fractions of METTL3 in *Dicer* knockdown and control HeLa cells. PARP-1 and β-Tubulin are used as nuclear and cytoplasmic markers, respectively.

(E and F) Blot (E) and quantitative analysis (F) of RNAs pulled down by Myc-METTL3 in the control and *Dicer* knockdown HeLa cells.

(legend continued on next page)

regulation of m^{6}A formation in both mouse and human cells by their mediation of the binding of METTL3 on mRNAs. These findings revealed a role of miRNAs in regulating mRNA epitranscriptomic modification in eukaryotes. Our findings on the functions of m^{6}A in cell reprogramming also suggested that modulating m^{6}A may serve as a strategy to regulate cell reprogramming.

EXPERIMENTAL PROCEDURES

Generation of iPSCs and Reprogramming Efficiency Evaluation

Generation of pluripotent iPSC lines was performed as described previously (Wernig et al., 2008). MEFs were isolated from E13.5 embryos heterozygous for the Oct4::GFP transgenic allele, as previously described (Huangfu et al., 2008), and cultured under established iPSC conditions with the four Yamanaka factors (*Oct4*, *Sox2*, *Klf4*, and *c-Myc*) expressed. The efficiency of iPSC formation is estimated according to the number of Oct4-GFP-positive colonies. GFP-positive colonies after 15 days of reprogramming were trypsinized and then analyzed using a FACS Calibur (BD Biosciences). A minimum of 10,000 events were recorded. Detection of alkaline phosphatase, which is an indicator of undifferentiated ESCs, was carried out after 15 days of reprogramming. The number of iPSC colonies per well was counted in triplicates. The expression of key pluripotent factors *Oct4*, *Sox2*, and *Nanog* was detected by qRT-PCR.

m^{6}A-seq Library Generation and Sequencing

m^{6}A immunoprecipitation and library construction procedure were modified from published procedure (Meyer et al., 2012). In brief, fragmented and ethanol precipitated mRNA (3 μg) from different cell lines was incubated with 5 μg of anti-m^{6}A polyclonal antibody (Synaptic Systems, 202003) in IPP buffer (150 mM NaCl, 0.1% NP-40, and 10 mM Tris-HCl [pH 7.4]) for 2 hr at 4°C. The mixture was then immunoprecipitated by incubation with 50 μl protein-A beads (Sigma, P9424) at 4°C for an additional 2 hr. After being washed three times, bound RNA was eluted from the beads with 0.5 mg/ml N^6-methyladenosine (BERRY & ASSOCIATES, PR3732) in IPP buffer and then extracted by Trizol. The remaining RNA was re-suspended in H_2O and used for library generation with mRNA sequencing kit (Illumina). Sequencing was carried out using the RNA-seq method as described in the Supplemental Procedures.

Sequencing Data Processing and m^{6}A Peak Calling

Sequence reads were mapped to the mouse reference genome (mm9) using TopHat (version 2.0.4) with a RefSeq-based transcript index (Kim et al., 2013). For RNA-seq analysis, the expression of transcripts was quantified as Fragments Per Kilobase of transcript per Million mapped reads (FPKM) and estimated by Cufflinks (version 2.0.2) (Trapnell et al., 2013). Cell-type-specific transcripts were identified using the Shannon entropy of each transcript following the previously reported method (Xie et al., 2013). To identify m^{6}A-enriched regions (m^{6}A peaks), the normalized values of Reads Per Kilobase of genome per Million mapped reads (RPKM) of both mapped m^{6}A-seq reads and RNA-seq reads were calculated and used. m^{6}A peaks were identified by the comparison of the read abundance between m^{6}A-seq and RNA-seq samples of the same loci with a method modified from a previous report (Meyer et al., 2012). Briefly, the entire mouse genome was divided into 25 nt bins and the numbers of both m^{6}A-seq reads and RNA-seq reads (used as control) mapped to each bin were counted and compared. Bins with statistically enriched m^{6}A-seq reads as compared to the RNA-seq reads (adjusted $p \leq 0.01$, Fisher's exact test together with Benjamini-Hocberg procedure) were identified and concatenated adjacently. m^{6}A-seq reads enriched regions with lengths no less than 75 nts were kept as m^{6}A peaks. m^{6}A peaks longer than 200 nts were split into 200 nt smaller peaks during the total m^{6}A peak counting process. Using the same criteria, regions statistically enriched for RNA-seq reads were chosen as the control peaks. The m^{6}A peaks of human HeLa cells were identified using the same criteria with data from the GEO database GSE46705.

Motif Identification among m^{6}A Peaks

Sequence motifs enriched in m^{6}A peaks were identified by HOMER with m^{6}A peaks as the target sequences and control peaks as the background using default parameters (Heinz et al., 2010) and visualized using WebLogo (Crooks et al., 2004). The enriched motifs were randomly shuffled to generate 500 groups of simulated motifs in each cell type and were used for specificity analysis.

Relationship Analysis of miRNAs with m^{6}A Peaks

Mouse mature miRNA sequences were downloaded from miRBase (Release 20 with 1,908 mouse miRNA sequences) (Kozomara and Griffiths-Jones, 2011), then compared with the motifs identified by HOMER or randomly simulated motifs using in-house scripts. miRNAs with seed regions (5′ 2-8 nts) reverse complementarily pairing (with at most one mismatch) to m^{6}A motifs were selected. To compare miRNA sequences with all m^{6}A peaks, the entire sequences of identified m^{6}A peaks and control peaks were extracted and paired with the miRNA sequences using miRanda software with "−sc 155 −en −20" and other default settings as parameters (Enright et al., 2003). m^{6}A peak sequences and control peak sequences that passed the above criteria were identified as miRNA-targeted peaks.

m^{6}A Manipulation during the iPSC Process

Under the iPSC induction condition as described above, the following experiments were carried out from the first day of reprogramming. In the *METTL3* overexpression experiments, 5 μg of plasmids expressing pCMV-Myc-*METTL3* and 5 μg pCMV-Myc-control plasmids were transfected into MEFs using Lipofectamine 2000 kit (Invitrogen) three times every 3 days. In the *METTL3* knockdown experiment, 75 nM siRNAs targeting *METTL3* and 75 nM control siRNAs were transfected into MEFs using Lipofectamine RNAiMAX (Invitrogen) four times every 3 days. In the rescue experiment, 5 μg of plasmids expressing pCMV-Myc-*hMETTL3* (Ping et al., 2014), which does not contain the target site of mouse *METTL3* siRNAs, and 5 μg of control plasmids were transfected into the *METTL3* knockdown MEFs three times every 3 days. In the chemical m^{6}A inhibition experiments, 20 mM cycloleucine was added to the culture medium of MEFs once per day for 10 days.

Statistical Analysis

Student's t test was used for all statistical analyses for experimental results (unless stated otherwise).

See Supplemental Experimental Procedures for a full description of the methods.

ACCESSION NUMBERS

Sequencing data generated by this work have been deposited into the Gene Expression Omnibus (GEO; accession number GSE52125).

(G) METTL3-RIP-qRT-PCR showing the changes of METTL3 binding at predicted target sites (DGCR2 and TUBB4B) of overexpressed (OE-miR) and repressed (anti-miR) miRNAs. Non-target regions (TXNRD1 and CTNNA1) of the operated miRNAs were used as controls.

(H) Western blot analysis showing equal amounts of METTL3 in control cells, miRNA-overexpression HeLa cells, and miRNA-knockdown HeLa cells (left panel) and comparable METTL3 immunoprecipitation efficiency (right panel).

(I) Blot analysis of RNAs pulled down by Myc-METTL3 in the control and *Dicer* knockdown mouse NSC cells. β-Tubulin is used as a loading control.

(J) METTL3-RIP-qRT-PCR showing the changes of METTL3 binding at predicted target sites (TCF4 and RPS13) of overexpressed (OE-miR) and repressed (anti-miR) miRNAs. A non-target region of miRNAs (EEF1A1) is used as a control.

Values and error bars in all bar plots represent the mean and SD of three independent experiments. *$p < 0.05$, **$p < 0.01$, and ***$p < 0.001$ by Student's t test. See also Figure S5 and Table S6.

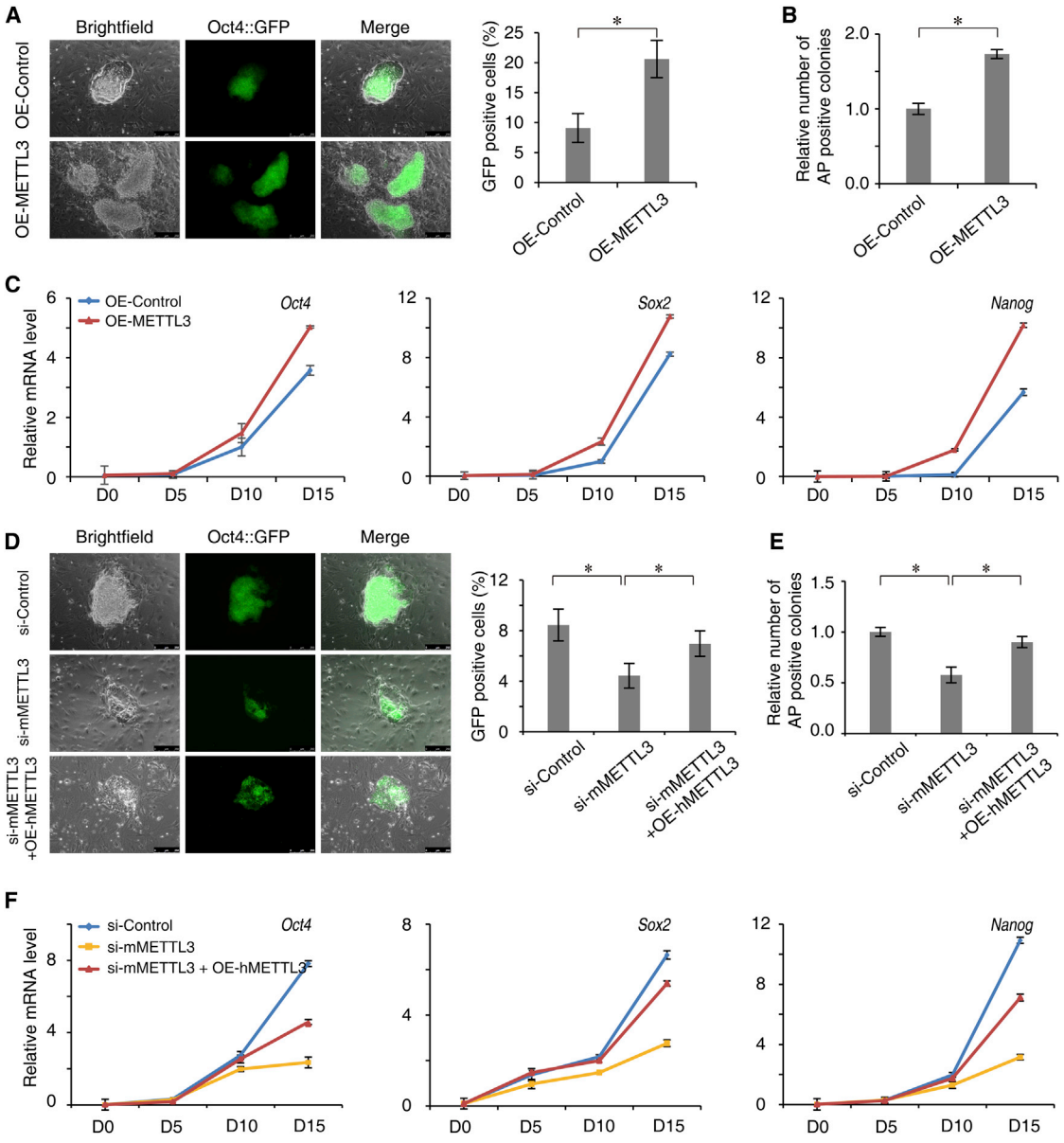

Figure 6. Modulating m^{6}A Abundance by METTL3 Regulates Cell Reprogramming

(A) Morphology (left panel) and quantitative (right panel) analysis of Oct4-GFP-positive clones among reprogrammed MEFs with control vector (OE-Control) and mouse *METTL3* overexpression (OE-*METTL3*).

(B) AP-positive clones among reprogrammed MEFs with control vector (OE-Control) and mouse *METTL3* overexpression (OE-*METTL3*).

(C) The expression levels (detected by qRT-PCR) of endogenous *Oct4*, *Sox2*, and *Nanog* in cells during the reprogramming process of MEFs with the control vector (OE-Control) and mouse *METTL3* overexpression (OE-*METTL3*).

(D) Morphology (left panel) and quantitative (right panel) analysis of Oct4-GFP-positive clones among reprogrammed MEFs with control siRNAs (si-Control), siRNAs for mouse *METTL3* (si-m*METTL3*), and human Myc-*METTL3* rescue (si-m*METTL3*+OE-h*METTL3*).

(E) AP-positive clones among reprogrammed MEFs with control siRNAs (si-Control), siRNAs for mouse *METTL3* (si-m*METTL3*), and human Myc-*METTL3* rescue (si-m*METTL3*+OE-h*METTL3*).

(F) The expression levels (detected by qRT-PCR) of endogenous *Oct4*, *Sox2*, and *Nanog* in cells during the reprogramming process of MEFs with control siRNAs (si-Control), siRNAs for mouse *METTL3* (si-m*METTL3*), and human Myc-*METTL3* rescue (si-m*METTL3*+OE-h*METTL3*).

Values and error bars in all plots represent the mean and SD of three independent experiments. *$p < 0.05$ by Student's t test. See also Figure S6 and Table S6.

SUPPLEMENTAL INFORMATION

Supplemental Information for this article includes six figures, six tables, and Supplemental Experimental Procedures and can be found with this article online at http://dx.doi.org/10.1016/j.stem.2015.01.016.

AUTHOR CONTRIBUTIONS

Q.Z., Y.Y., and X.W. conceived this project, supervised the experiments, analyzed data, and wrote the manuscript. T.C. and X.W. performed bioinformatics analysis, prediction, experimental candidates selection, and

experimental results analysis; Y.H. and M.L. did the m^{6}A cellular analysis; Y.Z. did the stem cell analysis; Y.Z., W.H, J.H., L.W., Y.L., and L.S. performed stem cell culture and cell reprogramming experiments; and Y.H., M.L., M.W., Y.W., Y.L., A.L., Y.Y., K.J., X.Z., X.P., W.L., L.W., G.J., and H.W. performed molecular biology experiments. T.C. and Y.Z. were also involved in molecular biology experiments.

ACKNOWLEDGMENTS

This work was supported by China 973 programs (2011CBA01101 to Q.Z. and X.-J.W. and 2014CB964900 to X.-J.W.); CAS Strategic Priority Research Program Grants XDA01020101 (to Q.Z.), XDA01020105 (to X.-J.W.), and XDB14030300 (to Y.-G. Y.); and the National Natural Science Foundation of China (91319308 to Q.Z. and 31430022 and 31370796 to Y.-G.Y.). We thank BIG sequencing core facility for sequencing.

Received: November 1, 2013
Revised: September 30, 2014
Accepted: January 28, 2015
Published: February 12, 2015

REFERENCES

Bartel, D.P. (2004). MicroRNAs: genomics, biogenesis, mechanism, and function. Cell *116*, 281–297.

Batista, P.J., Molinie, B., Wang, J., Qu, K., Zhang, J., Li, L., Bouley, D.M., Lujan, E., Haddad, B., Daneshvar, K., et al. (2014). m(6)A RNA modification controls cell fate transition in mammalian embryonic stem cells. Cell Stem Cell *15*, 707–719.

Bodi, Z., Button, J.D., Grierson, D., and Fray, R.G. (2010). Yeast targets for mRNA methylation. Nucleic Acids Res. *38*, 5327–5335.

Bodi, Z., Zhong, S., Mehra, S., Song, J., Graham, N., Li, H., May, S., and Fray, R.G. (2012). Adenosine methylation in Arabidopsis mRNA is associated with the 3′ end and reduced Levels cause developmental defects. Front. Plant Sci. *3*, 48.

Bokar, J.A. (2005). The biosynthesis and functional roles of methylated nucleosides in eukaryotic mRNA, Volume 12, H. Grosjean, ed. (New York: Springer), pp. 141–177.

Bokar, J.A., Shambaugh, M.E., Polayes, D., Matera, A.G., and Rottman, F.M. (1997). Purification and cDNA cloning of the AdoMet-binding subunit of the human mRNA (N6-adenosine)-methyltransferase. RNA *3*, 1233–1247.

Camper, S.A., Albers, R.J., Coward, J.K., and Rottman, F.M. (1984). Effect of undermethylation on mRNA cytoplasmic appearance and half-life. Mol. Cell. Biol. *4*, 538–543.

Cantara, W.A., Crain, P.F., Rozenski, J., McCloskey, J.A., Harris, K.A., Zhang, X., Vendeix, F.A., Fabris, D., and Agris, P.F. (2011). The RNA modification database, RNAMDB: 2011 update. Nucleic Acids Res. *39*, D195–D201.

Cenik, E.S., and Zamore, P.D. (2011). Argonaute proteins. Curr. Biol. *21*, R446–R449.

Crooks, G.E., Hon, G., Chandonia, J.M., and Brenner, S.E. (2004). WebLogo: a sequence logo generator. Genome Res. *14*, 1188–1190.

Dai, Q., Fong, R., Saikia, M., Stephenson, D., Yu, Y.T., Pan, T., and Piccirilli, J.A. (2007). Identification of recognition residues for ligation-based detection and quantitation of pseudouridine and N6-methyladenosine. Nucleic Acids Res. *35*, 6322–6329.

Desrosiers, R., Friderici, K., and Rottman, F. (1974). Identification of methylated nucleosides in messenger RNA from Novikoff hepatoma cells. Proc. Natl. Acad. Sci. USA *71*, 3971–3975.

Dominissini, D., Moshitch-Moshkovitz, S., Schwartz, S., Salmon-Divon, M., Ungar, L., Osenberg, S., Cesarkas, K., Jacob-Hirsch, J., Amariglio, N., Kupiec, M., et al. (2012). Topology of the human and mouse m6A RNA methylomes revealed by m6A-seq. Nature *485*, 201–206.

Enright, A.J., John, B., Gaul, U., Tuschl, T., Sander, C., and Marks, D.S. (2003). MicroRNA targets in Drosophila. Genome Biol. *5*, R1.

Finkel, D., and Groner, Y. (1983). Methylations of adenosine residues (m6A) in pre-mRNA are important for formation of late simian virus 40 mRNAs. Virology *131*, 409–425.

Fustin, J.M., Doi, M., Yamaguchi, Y., Hida, H., Nishimura, S., Yoshida, M., Isagawa, T., Morioka, M.S., Kakeya, H., Manabe, I., and Okamura, H. (2013). RNA-methylation-dependent RNA processing controls the speed of the circadian clock. Cell *155*, 793–806.

Geula, S., Moshitch-Moshkovitz, S., Dominissini, D., Mansour, A.A., Kol, N., Salmon-Divon, M., Hershkovitz, V., Peer, E., Mor, N., Manor, Y.S., et al. (2015). m6A mRNA methylation facilitates resolution of naïve pluripotency toward differentiation. Science, in press. Published online January 1, 2015. http://dx.doi.org/10.1126/science.1261417.

Globisch, D., Pearson, D., Hienzsch, A., Brückl, T., Wagner, M., Thoma, I., Thumbs, P., Reiter, V., Kneuttinger, A.C., Müller, M., et al. (2011). Systems-based analysis of modified tRNA bases. Angew. Chem. Int. Ed. Engl. *50*, 9739–9742.

Harper, J.E., Miceli, S.M., Roberts, R.J., and Manley, J.L. (1990). Sequence specificity of the human mRNA N6-adenosine methylase in vitro. Nucleic Acids Res. *18*, 5735–5741.

He, C. (2010). Grand challenge commentary: RNA epigenetics? Nat. Chem. Biol. *6*, 863–865.

Heinz, S., Benner, C., Spann, N., Bertolino, E., Lin, Y.C., Laslo, P., Cheng, J.X., Murre, C., Singh, H., and Glass, C.K. (2010). Simple combinations of lineage-determining transcription factors prime cis-regulatory elements required for macrophage and B cell identities. Mol. Cell *38*, 576–589.

Hess, M.E., Hess, S., Meyer, K.D., Verhagen, L.A., Koch, L., Brönneke, H.S., Dietrich, M.O., Jordan, S.D., Saletore, Y., Elemento, O., et al. (2013). The fat mass and obesity associated gene (Fto) regulates activity of the dopaminergic midbrain circuitry. Nat. Neurosci. *16*, 1042–1048.

Huangfu, D., Maehr, R., Guo, W., Eijkelenboom, A., Snitow, M., Chen, A.E., and Melton, D.A. (2008). Induction of pluripotent stem cells by defined factors is greatly improved by small-molecule compounds. Nat. Biotechnol. *26*, 795–797.

Jia, G., Fu, Y., Zhao, X., Dai, Q., Zheng, G., Yang, Y., Yi, C., Lindahl, T., Pan, T., Yang, Y.G., and He, C. (2011). N6-methyladenosine in nuclear RNA is a major substrate of the obesity-associated FTO. Nat. Chem. Biol. *7*, 885–887.

Kane, S.E., and Beemon, K. (1985). Precise localization of m6A in Rous sarcoma virus RNA reveals clustering of methylation sites: implications for RNA processing. Mol. Cell. Biol. *5*, 2298–2306.

Kim, D., Pertea, G., Trapnell, C., Pimentel, H., Kelley, R., and Salzberg, S.L. (2013). TopHat2: accurate alignment of transcriptomes in the presence of insertions, deletions and gene fusions. Genome Biol. *14*, R36.

Kozomara, A., and Griffiths-Jones, S. (2011). miRBase: integrating microRNA annotation and deep-sequencing data. Nucleic Acids Res. *39*, D152–D157.

Liu, J., and Jia, G. (2014). Methylation modifications in eukaryotic messenger RNA. J. Genet. Genomics *41*, 21–33.

Liu, N., Parisien, M., Dai, Q., Zheng, G., He, C., and Pan, T. (2013). Probing N6-methyladenosine RNA modification status at single nucleotide resolution in mRNA and long noncoding RNA. RNA *19*, 1848–1856.

Liu, J., Yue, Y., Han, D., Wang, X., Fu, Y., Zhang, L., Jia, G., Yu, M., Lu, Z., Deng, X., et al. (2014). A METTL3-METTL14 complex mediates mammalian nuclear RNA N6-adenosine methylation. Nat. Chem. Biol. *10*, 93–95.

Machnicka, M.A., Milanowska, K., Osman Oglou, O., Purta, E., Kurkowska, M., Olchowik, A., Januszewski, W., Kalinowski, S., Dunin-Horkawicz, S., Rother, K.M., et al. (2013). MODOMICS: a database of RNA modification pathways—2013 update. Nucleic Acids Res. *41*, D262–D267.

Meister, G. (2013). Argonaute proteins: functional insights and emerging roles. Nat. Rev. Genet. *14*, 447–459.

Meyer, K.D., Saletore, Y., Zumbo, P., Elemento, O., Mason, C.E., and Jaffrey, S.R. (2012). Comprehensive analysis of mRNA methylation reveals enrichment in 3′ UTRs and near stop codons. Cell *149*, 1635–1646.

Niu, Y., Zhao, X., Wu, Y.S., Li, M.M., Wang, X.J., and Yang, Y.G. (2013). N6-methyl-adenosine (m6A) in RNA: an old modification with a novel epigenetic function. Genomics Proteomics Bioinformatics *11*, 8–17.

Ping, X.L., Sun, B.F., Wang, L., Xiao, W., Yang, X., Wang, W.J., Adhikari, S., Shi, Y., Lv, Y., Chen, Y.S., et al. (2014). Mammalian WTAP is a regulatory subunit of the RNA N6-methyladenosine methyltransferase. Cell Res. *24*, 177–189.

Rand, T.A., Petersen, S., Du, F., and Wang, X. (2005). Argonaute2 cleaves the anti-guide strand of siRNA during RISC activation. Cell *123*, 621–629.

Schwartz, S., Agarwala, S.D., Mumbach, M.R., Jovanovic, M., Mertins, P., Shishkin, A., Tabach, Y., Mikkelsen, T.S., Satija, R., Ruvkun, G., et al. (2013). High-resolution mapping reveals a conserved, widespread, dynamic mRNA methylation program in yeast meiosis. Cell *155*, 1409–1421.

Schwartz, S., Mumbach, M.R., Jovanovic, M., Wang, T., Maciag, K., Bushkin, G.G., Mertins, P., Ter-Ovanesyan, D., Habib, N., Cacchiarelli, D., et al. (2014). Perturbation of m6A writers reveals two distinct classes of mRNA methylation at internal and 5′ sites. Cell Rep. *8*, 284–296.

Sibbritt, T., Patel, H.R., and Preiss, T. (2013). Mapping and significance of the mRNA methylome. Wiley Interdiscip Rev RNA *4*, 397–422.

Trapnell, C., Hendrickson, D.G., Sauvageau, M., Goff, L., Rinn, J.L., and Pachter, L. (2013). Differential analysis of gene regulation at transcript resolution with RNA-seq. Nat. Biotechnol. *31*, 46–53.

Tuck, M.T., Wiehl, P.E., and Pan, T. (1999). Inhibition of 6-methyladenine formation decreases the translation efficiency of dihydrofolate reductase transcripts. Int. J. Biochem. Cell Biol. *31*, 837–851.

Wang, X., Lu, Z., Gomez, A., Hon, G.C., Yue, Y., Han, D., Fu, Y., Parisien, M., Dai, Q., Jia, G., et al. (2014a). N6-methyladenosine-dependent regulation of messenger RNA stability. Nature *505*, 117–120.

Wang, Y., Li, Y., Toth, J.I., Petroski, M.D., Zhang, Z., and Zhao, J.C. (2014b). N6-methyladenosine modification destabilizes developmental regulators in embryonic stem cells. Nat. Cell Biol. *16*, 191–198.

Wei, C.-M., and Moss, B. (1977). Nucleotide sequences at the N6-methyladenosine sites of HeLa cell messenger ribonucleic acid. Biochemistry *16*, 1672–1676.

Wei, C.M., Gershowitz, A., and Moss, B. (1975). Methylated nucleotides block 5′ terminus of HeLa cell messenger RNA. Cell *4*, 379–386.

Wernig, M., Lengner, C.J., Hanna, J., Lodato, M.A., Steine, E., Foreman, R., Staerk, J., Markoulaki, S., and Jaenisch, R. (2008). A drug-inducible transgenic system for direct reprogramming of multiple somatic cell types. Nat. Biotechnol. *26*, 916–924.

Xie, W., Schultz, M.D., Lister, R., Hou, Z., Rajagopal, N., Ray, P., Whitaker, J.W., Tian, S., Hawkins, R.D., Leung, D., et al. (2013). Epigenomic analysis of multilineage differentiation of human embryonic stem cells. Cell *153*, 1134–1148.

Xu, C., Wang, X., Liu, K., Roundtree, I.A., Tempel, W., Li, Y., Lu, Z., He, C., and Min, J. (2014). Structural basis for selective binding of m6A RNA by the YTHDC1 YTH domain. Nat. Chem. Biol. *10*, 927–929.

Zhao, X., Yang, Y., Sun, B.F., Shi, Y., Yang, X., Xiao, W., Hao, Y.J., Ping, X.L., Chen, Y.S., Wang, W.J., et al. (2014). FTO-dependent demethylation of N6-methyladenosine regulates mRNA splicing and is required for adipogenesis. Cell Res. *24*, 1403–1419.

Zheng, G., Dahl, J.A., Niu, Y., Fedorcsak, P., Huang, C.M., Li, C.J., Vågbø, C.B., Shi, Y., Wang, W.L., Song, S.H., et al. (2013). ALKBH5 is a mammalian RNA demethylase that impacts RNA metabolism and mouse fertility. Mol. Cell *49*, 18–29.

Zhong, S., Li, H., Bodi, Z., Button, J., Vespa, L., Herzog, M., and Fray, R.G. (2008). MTA is an Arabidopsis messenger RNA adenosine methylase and interacts with a homolog of a sex-specific splicing factor. Plant Cell *20*, 1278–1288.

Zhu, T., Roundtree, I.A., Wang, P., Wang, X., Wang, L., Sun, C., Tian, Y., Li, J., He, C., and Xu, Y. (2014). Crystal structure of the YTH domain of YTHDF2 reveals mechanism for recognition of N6-methyladenosine. Cell Res. *24*, 1493–1496.